Publications of the Astronomical Society of Australia (PASA)
doi: 10.1017/pas.2023.xxx.

The MeerKAT Telescope as a Pulsar Facility: System verification and early science results from MeerTime

M. Bailes[1,2]*, A. Jameson[1,2], F. Abbate[3,4,5], E. D. Barr[4], N. D. R. Bhat[6], L. Bondonneau[7,8], M. Burgay[3], S. J. Buchner[9], F. Camilo[9], D. J. Champion[4], I. Cognard[7,8], P. C. C. Freire[4], T. Gautam[4], M. Geyer[9], J.-M. Griessmeier[7,8], L. Guillemot[7,8] H. Hu[4], F. Jankowski[10], S. Johnston[11], A. Karastergiou[12], R. Karuppusamy[4], M. J. Keith[10], M. Kramer[4], J. van Leeuwen[13,14], M. E. Lower[1,11], Y. Maan[13], M. A. McLaughlin[15], B. W. Meyers[16,6], S. Osłowski[1], L. S. Oswald[12], A. Parthasarathy[1,2,4], B. Posselt[12,17], A. Possenti[3,18], S. M. Ransom[19], D. J. Reardon[1], A. Ridolfi[3,4], C. T. G. Schollar[9], M. Serylak[9,20], G. Shaifullah[13], M. Shamohammadi[1,2], R. M. Shannon[1,2], C. Sobey[21], X. Song[10], R. Spiewak[1,2], I. H. Stairs[16], B. W. Stappers[10], W. van Straten[22], A. Szary[13,23], G. Theureau[7,8], V. Venkatraman Krishnan[4], P. Weltevrede[10], N. Wex[4], T. D. Abbott[9], G. B. Adams[9], J. P. Burger[9], R. R. G. Gamatham[9], M. Gouws[9], D. M. Horn[9], B. Hugo[9,24], A. F. Joubert[9], J. R. Manley[9], K. McAlpine[9], S. S. Passmoor[9], A. Peens-Hough[9], Z. R. Ramudzuli[9], A. Rust[9], S. Salie[9], L. C. Schwardt[9], R. Siebrits[9], G. Van Tonder[9], V. Van Tonder[9], M. G. Welz[9]

[1] Centre for Astrophysics and Supercomputing, Swinburne University of Technology, P.O. Box 218, Hawthorn, VIC 3122, Australia
[2] ARC Centre of Excellence for Gravitational Wave Discovery (OzGrav)
[3] INAF - Osservatorio Astronomico di Cagliari, Via della Scienza 5, 09047 Selargius (CA), Italy
[4] Max-Planck-Institut für Radioastronomie, Auf dem Hügel 69, D-53121 Bonn, Germany
[5] Dipartimento di Fisica 'G. Occhialini', Università degli Studi Milano - Bicocca, Piazza della Scienza 3, 20126, Milano, Italy
[6] International Centre for Radio Astronomy Research (ICRAR), Curtin University, 1 Turner Avenue, Technology Park, Bentley, WA 6102, Australia
[7] Laboratoire de Physique et Chimie de l'Environnement et de l'Espace LPC2E CNRS-Université d'Orléans, F-45071 Orléans, France
[8] Station de radioastronomie de Nançay, Observatoire de Paris, PSL Research University, CNRS/INSU F-18330 Nançay, France
[9] South African Radio Astronomy Observatory, 2 Fir Street, Black River Park, Observatory 7925, South Africa
[10] Jodrell Bank Centre for Astrophysics, Department of Physics and Astronomy, The University of Manchester, Manchester M13 9PL, UK
[11] CSIRO Astronomy & Space Science, Australia Telescope National Facility, P.O. Box 76, Epping, NSW 1710, Australia
[12] Department of Astrophysics, University of Oxford, Denys Wilkinson Building, Keble Road, Oxford OX1 3RH, UK
[13] ASTRON, The Netherlands Institute for Radio Astronomy, Postbus 2, NL-7900 AA Dwingeloo, the Netherlands
[14] Anton Pannekoek Institute for Astronomy, University of Amsterdam, Science Park 904, 1098 XH Amsterdam, Netherlands
[15] Department of Physics and Astronomy, West Virginia University, Morgantown, WV 26506-6315 and the Center for Gravitational Waves and Cosmology, Morgantown, WV 26505
[16] Department of Physics and Astronomy, University of British Columbia, 6224 Agricultural Road, Vancouver, BC V6T 1Z1, Canada
[17] Department of Astronomy & Astrophysics, Pennsylvania State University, 525 Davey Lab, 16802 University Park, PA, USA
[18] Universitá di Cagliari, Dip di Fisica, S.P. Monserrato-Sestu Km 0,700 - 09042 Monserrato (CA), Italy
[19] National Radio Astronomy Observatory, 520 Edgemont Rd., Charlottesville, VA 22903, USA
[20] Department of Physics and Astronomy, University of the Western Cape, Bellville, Cape Town 7535, South Africa
[21] CSIRO Astronomy and Space Science, 26 Dick Perry Avenue, Kensington, WA 6151, Australia
[22] Institute for Radio Astronomy & Space Research, Auckland University of Technology, Private Bag 92006, Auckland 1142, NZ
[23] Janusz Gil Institute of Astronomy, University of Zielona Góra, Lubuska 2, 65-265 Zielona Góra, Poland
[24] Department of Physics and Electronics, Rhodes University, PO Box 94, Grahamstown 6140, South Africa

Abstract

We describe system verification tests and early science results from the pulsar processor (PTUSE) developed for the newly-commissioned 64-dish SARAO MeerKAT radio telescope in South Africa. MeerKAT is a high-gain ($\sim 2.8\,\mathrm{K/Jy}$) low-system temperature ($\sim 18\,\mathrm{K}$ at 20cm) radio array that currently operates from 580–1670 MHz and can produce tied-array beams suitable for pulsar observations. This paper presents results from both MeerKAT commissioning data and the MeerTime Large Survey Project with PTUSE. Highlights include observations of the double pulsar J0737−3039A, pulse profiles from 34 millisecond pulsars from a single 2.5 h observation of the Globular cluster Terzan 5, the rotation measure of Ter5O, a 420-sigma giant pulse from the Large Magellanic Cloud pulsar PSR J0540−6919, and nulling identified in the slow pulsar PSR J0633–2015 by virtue of MeerKAT's exceptional sensitivity. One of the key design specifications for MeerKAT was absolute timing errors of less than 5 ns using their novel precise time system. Our timing of two bright millisecond pulsars confirm that MeerKAT already delivers exceptional timing. PSR J2241−5236 exhibits a jitter limit of < 4 ns per hour during scintillation maxima whilst timing of PSR J1909−3744 over almost 11 months yields an rms residual of 66 ns with only 4 min integrations. Our results confirm that the MeerKAT is an exceptional pulsar telescope. The array can be split into four separate sub-arrays to time over 1000 pulsars per day and in the future the deployment of S-band (1750–3500 MHz) receivers will further enhance its capabilities.

1 INTRODUCTION

In the standard model, radio pulsars are highly-magnetised rapidly rotating neutron stars that emit a coherent beam of often highly polarised radio emission along their magnetic poles (Lorimer & Kramer, 2004). The weak braking torques caused by their rapidly rotating magnetic fields and their high moments of inertia make them extremely stable flywheels, and it is often possible to predict the pulsar spin period and indeed pulse phase years in advance of observation (Taylor, 1992). Most radio pulsars regularly emit irregular single-pulse shapes that usually sum to an average profile within 1000 rotations that is often remarkably constant (Liu et al., 2012). Timing of these mean profiles against a template produces an arrival time which can be used to derive a model of the pulsar's spin-down, astrometric and binary parameters and propagation through the ionised interstellar medium. The frequency-dependence of the pulse arrival time is well described by the cold plasma dispersion relation, and allows observers to compute the column density of free electrons along the line of sight to the observer.

State of the art pulsar timing allows us to measure pulse arrival times to better than one part in 10^4 of pulse period (van Straten et al., 2001), leading to sub-microsecond arrival times for the fastest (millisecond) pulsars. In their most recent data release (dr2) the International Pulsar Timing Array[1] lists an rms timing residual for the bright millisecond pulsar (MSP) PSR J0437−4715 of just 110 ns and 14 others with residuals below 1 μs (Perera et al., 2019).

According to version 1.62 (Feb 2020) of the ATNF pulsar catalogue[2] (Manchester et al., 2005) there are currently 2800 pulsars known, $\sim 97\%$ of which are visible at radio wavelengths. Radio pulsars range in pulse period from 1.4 ms to 23.5 s, and have inferred dipolar magnetic field strengths from 5×10^7G to $\sim10^{15}$ G. Over 10 percent of known pulsars are members of binary systems, and the majority of these are the so-called 'recycled pulsars', that have had their magnetic fields weakened and spin periods shortened by mass accretion from a donor. These pulsars are often in very clean systems well approximated by point masses and ideal for tests of gravitational theories and stellar evolution models (Weisberg & Huang, 2016).

Modern radio telescopes can detect radio pulsars with a mean flux density (ie averaged over the pulse period) down to just a few μJy in very deep pointings, and the large-scale surveys of much of the galactic plane are complete to $\sim$0.1 mJy (Ng et al., 2015). The population exhibits a standard log-N/log-S distribution consistent with a largely planar distribution with a slope of ~ -1. The most compelling pulsar science is usually derived from accurate pulse timing which for most pulsars is signal-to-noise limited as the vast majority of known pulsars have flux densities less than 1 mJy at 1400 MHz. For this reason the field has been dominated by the world's largest radio telescopes that possess low-temperature receivers and digital backends capable of coherently dedispersing the voltages induced in the receiver by the radio pulsars. These telescopes can produce the high signal-to-noise profiles required to test theories of relativistic gravity, determine neutron star masses, clarify the poorly-understood radio emission mechanism, and relate the latter to the magnetic field topology.

The galactic centre is at declination $\delta = -29°$ and this makes the Southern hemisphere a particularly inviting location for pulsar studies. For many years the Parkes 64 m telescope has had almost exclusive access to radio pulsars south of declination $\delta = -35°$, and consequently discovered the bulk of the pulsar population. When choosing a site and host country for the forthcoming Square Kilometre Array SKA1-mid telescope, the strong pulsar science case made Southern hemisphere locations particularly desirable. MeerKAT is the South African SKA precursor telescope located at the future site of SKA1-mid and the full array has four times the gain (i.e. 2.8 K/Jy) of the Parkes telescope (0.7 K/Jy). The first receivers (L-band) to come online has an excellent system temperature ($\sim$18 K) along with 856 MHz of recorded bandwidth. The pulsar processor often just records the inner 776 MHz of this for science purposes. The telescope is located at latitude $-30°43'$ and is ideal for studies of the large population of southern pulsars and those in the Large and Small Magellanic Clouds. Much of pulsar science is signal-to-noise limited until a pulsar hits its 'jitter limit' (the lowest timing residual obtainable due to pulse-to-pulse variability in the individual pulses), timing accuracy is proportional to the signal to noise ratio obtainable. For most pulsars in the Parkes Pulsar Timing Array (Manchester et al., 2013), the limit is rarely reached when observed with the Parkes 64 m telescope unless the pulsar is experiencing a scintillation maximum (Shannon et al., 2014). A notable exception is the bright MSP PSR J0437–4715, that is always jitter-limited when observed at the Parkes telescope (Osłowski et al., 2011) due to its large 1400 MHz mean flux density of 150 mJy (Dai et al., 2015). As telescopes become more sensitive, the number of pulsars in the same integration time being jitter-limited increases.

The South African Radio Astronomy Observatory (SARAO) owns and operates MeerKAT and, before it was commissioned, called for Large Survey Projects (LSPs) that could exploit the telescope's scientific potential. The MeerTime[3] (Bailes et al., 2018) collaboration was successful at obtaining LSP status and commenced its first survey observations in February of 2019. This

*mbailes@swin.edu.au

[1] www.ipta4gw.org

[2] https://www.atnf.csiro.au/research/pulsar/psrcat/

[3] http://www.meertime.org

paper reports on MeerTime's validation of MeerKAT as a pulsar telescope and presents some early science results from its four major themes: Relativistic and Binary Pulsars, the Thousand Pulsar Array (Johnston, 2020), Globular Clusters and the MeerKAT Pulsar Timing Array.

A glimpse of MeerKAT's potential as a pulsar telescope was presented in (Camilo et al., 2018) when it was part of a campaign that observed the revival of the magnetar PSR J1622–4950. Since then there have been a number of developments of the system that enable a wider range of pulsar observing modes that will be discussed forthwith.

The structure of this paper is as follows. In section 2, we provide an overview of MeerKAT as a pulsar telescope including examples of the UHF and L-band radio bands, the Precise Time Manager (PTM), choice of polyphase filterbanks, and the SKA1 prototype pulsar processor PTUSE developed by Swinburne University of Technology. In section 3, we describe our validation of the system and pulsar hardware before presenting new science from observations of selected pulsars and globular clusters in section 4. Finally, we briefly discuss some of the prospects for the future of this facility including new modes, receivers, and extensions and ultimate extension to become SKA1-mid in section 5.

2 THE MEERKAT TELESCOPE AS A PULSAR FACILITY

2.1 The MeerKAT Radio Frequency Spectrum

MeerKAT is located in the Karoo, some 450 km northeast of Cape Town in the Northern Cape Province. Its low population density makes it an attractive site to pursue radio astronomy. The low-frequency HERA experiment (DeBoer et al., 2017) and the future 197-dish SKA1-mid telescope (Dewdney et al., 2009) – of which MeerKAT will be a part – will be located at the site which is protected by legislation against radio transmissions in many bands of relevance to astronomers.

The technology behind low-noise amplifiers and radio receivers has greatly improved since the dawn of radio astronomy in the 1950s. Whilst even just a couple of decades ago it was necessary to sacrifice fractional bandwidth to minimise system temperature new engineering practices and technologies now permit the development of low-noise (∼20 K) receivers over a full octave or more of bandwidth eg. (Hobbs et al., 2019).

The original MeerKAT specification had a target effective collecting area per unit receiver temperature of $A_{\rm eff}/T = 220$ m^2/K but remarkably achieved 350–450 m^2/K (depending upon radio frequency), well over a factor of 2 increase in observing efficiency over the design specification. These figures equate to a system equivalent flux density (SEFD) of SEFD $= T/G \sim 7$ Jy, where T is the system temperature in K and G is the total antenna gain $G = A\eta/(2k)$, where A is the collecting area, η is the aperture efficiency and k is Boltzmann's constant. The total MeerKAT antenna gain is 2.8 K/Jy and the system temperature about 18 K in the optimal location of the 1400 MHz band. The receivers have two orthogonal linear polarisations (H and V).

In Figure 1 we present the radio spectrum as observed from the MeerKAT site for the UHF (544–1088 MHz) and L-band (856–1712 MHz) receivers as well as integrated pulse profiles for the double pulsar PSR J0737−3039A at the same frequencies. Pulsar observations are usually made with 1024 or 4096 frequency channels being produced by the F-engines that are passed to the beam-former. The UHF band is remarkably clean, with just some small (time-dependent) residual phone transmissions visible around 940 MHz. In most countries that house large-diameter (64m class and above) telescopes, the UHF band is so badly polluted by digital television and mobile phone transmissions that it is often unusable except in very narrow windows some 10s of MHz wide. Both of the SKA sites appear to have been chosen well and offer a renewed opportunity to explore the Universe at these frequencies. For pulsars, this is especially relevant, as most possess steep spectra (Toscano et al., 1998; Maron et al., 2000; Jankowski et al., 2018), with spectral indices of between −1 and −3 above 1 GHz.

The 1400-MHz (L-band) receiver band is not as pristine as the UHF band, but still has much of the spectrum available for science (see a quantified analysis below), depending upon the flux density of the target pulsar. The tied-array beam helps dilute interfering signals by dephasing them but the large number of bits in the digitizers and beam-former that deliver accurate channelisation of the data have one drawback in the sense that the interference-to-noise ratio can be extremely high. This makes deletion of at least some frequency channels essential before integration across frequency channels.

Like all modern observatories, the 1400 MHz band suffers from transmissions from Global Navigation Satellite Systems (GNSS) and other satellites that are extremely strong and impossible to avoid. The small dishes (and hence large side-lobes) that the 14-m dishes of MeerKAT provide make satellite transmissions in the band almost omnipresent. The L-band spectrum is shown in Fig 1c.

To quantify the effect of radio frequency interference (RFI) on our pulsar science, we took observations of the narrow duty-cycle MSP PSR J1909−3744 from Feb 2019 until Nov 2019 and eliminated interference by looking for deviations in the pulsar's baseline that exceeded 5 sigma after averaging the pulse profile every 8 seconds. In total, we analysed 2825 8-second integrations. These results are shown in Figure 2. In the central 928 channels of the

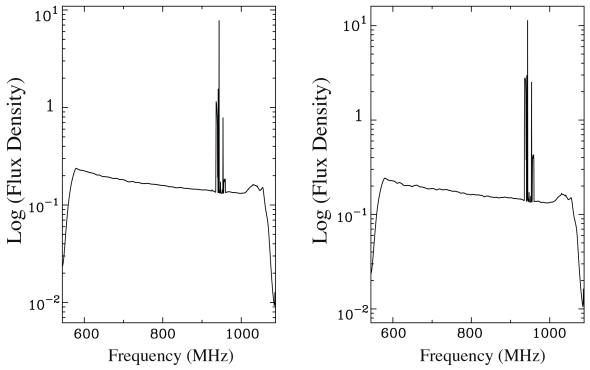

(a) Bandpasses from the H (left) and V (right) polarisations in the UHF band.

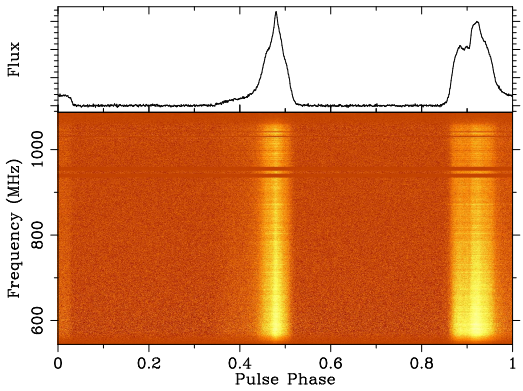

(b) Integrated pulse profile for PSR J0737-3039A with the UHF receiver. The flux density scale is arbitrary.

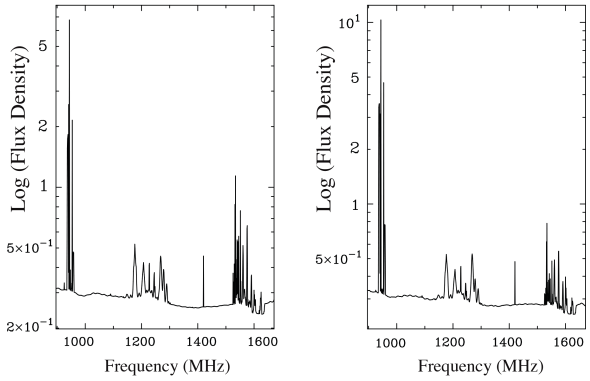

(c) Bandpasses from the H (left) and V (right) polarisations for the 1400 MHz band. Note that only the inner 928 channels of 1024 are presented hence the lack of roll-off of the band.

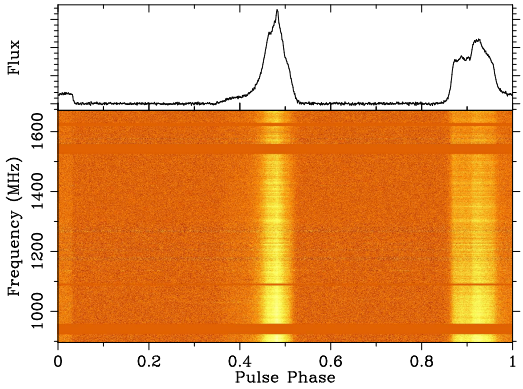

(d) Integrated pulse profile for PSR J0737-3039A with the L-band receiver. The flux density scale is arbitrary.

Figure 1. Observations of PSR J0737-3039A with MeerKAT's UHF and L-Band receivers.

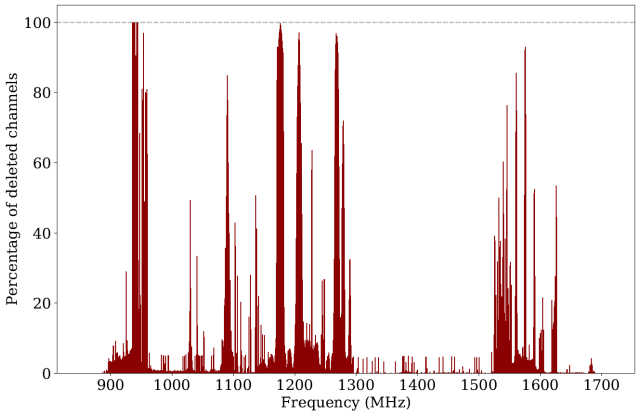

Figure 2. The fraction of 8-second folded integrations on PSR J1909−3744 where the baseline had an integrated boxcar greater than $5\,\sigma$ from the mean and were consequently deleted between Feb-Nov 2019 using the L-Band receiver.

1024 produced by the F-engines we only had to delete 12.8% of the 1400 MHz band, on average. Although, some of these channels have very persistent RFI and their deleted fraction is close to 100%.

On short timescales, the fraction of affected integrations is similar. In an analysis of a 7200-second observation of the giant-pulse emitting pulsar PSR J0540−6919 (Johnston & Romani, 2003), we created single pulse timing archives with an approximate integration time of 50.6 ms. We followed the same procedure we used for the PSR J1909−3744 observations to delete RFI-affected frequency channels. Single-pulse integrations make weaker RFI easier to detect as it is not washed out by the process of pulsar folding but also means RFI with an on/off timescale greater than (in this case) 50 ms can lead to integrations with less or almost no RFI. We found that, in a single two-hour observation, 9.6% of the band was deleted using the same criteria as for the integrated pulse profile tests.

To place these results in context, for much of the last two decades, observations at the Parkes 64 m telescope have used bandwidths of 256-340 MHz in the 20-cm band. Our results suggest that, for pulsar timing and single-pulse studies, effectively 87-90% of the 928 central frequency channels can be used for a total bandwidth of 675-700 MHz centred at 1400 MHz. This is very competitive with almost all existing large-aperture telescopes and comparable to the fraction of the 1400 MHz band at the NRAO Green Bank telescope (GBT) and only exceeded by the recent development of the Ultra-Wideband receiver (Hobbs et al., 2019) at the Parkes telescope that operates from 704 MHz to 4.032 GHz.

The first of the S-band ($1.75 - 3.5$ GHz) receivers of the Max-Planck-Institut für Radioastronomie (Kramer et al., 2016) are currently being installed and tested. When fully installed these will provide the possibility of performing high precision timing at higher frequencies.

2.2 Precise Time Systems in MeerKAT

2.2.1 Background on requirements

The SKA phase I (comprising SKA1-low and SKA1-mid) has been strongly motivated by two key science projects, the Epoch of Reionisation and strong-field tests of gravity respectively (e.g., Kramer et al., 2016). Despite the advent of direct gravitational wave detection and black hole imaging, a number of precision strong-field tests can only be achieved at radio wavelengths using pulsars. This includes the detection of a gravitational wave background from supermassive black holes using pulsar timing arrays, which will require timing an ensemble of MSPs to precisions well below 100 ns and possibly down to 10 ns. In order to achieve such precisions, two of the SKA1 specifications are especially relevant, one related to the calibration of the polarimetry that otherwise leads to systematic errors in timing; see, e.g., (Foster et al., 2015), and the other the knowledge of absolute time with respect to Coordinated Universal Time (UTC) over a full decade. The SKA1-mid specification on calibratable polarisation purity is −40 db, and on time 5 ns over 10 years.

The precise time systems in MeerKAT are specified to provide time products accurate to better than 5 ns, relative to UTC. Unique too is that the telescope was designed for absolute timing, not just relative timing which is the norm. This is achieved via a first-principles approach, by managing the time delays associated with every element of the geometric and signal paths.

2.2.2 Realisation of system timing for the MeerKAT telescope

MeerKAT has defined a reference point on the Earth to which all time is referred. It is a location a few hundred metres approximately north of the centre of the array and listed in the relevant TEMPO2 file with ECEF (Earth-centred, Earth-fixed) coordinates X=5109360.133, Y=2006852.586, Z=−3238948.127 m. The position of the reference point was chosen as the circumcentre of the array, roughly a metre above the ground. There is no antenna at this point; all pulsar timing is ultimately referred to when an incident radio wave would have struck this point.

The coordinates of the source, antenna and UT1 (where the Earth is pointing) define the geometric delay, and every attempt is made to derive the further delays incurred by the signal as it reflects off the telescope surfaces, passes through the feed/receiver/cable/filter and is ultimately sampled by the analogue to digital converters (ADCs). Round-trip measurements account for cable and fibre delays and are accurate to 1 ns. Estimates of the error in each stage of the path are also recorded for later dissemination to the pulsar processor to be recorded with the data.

At each antenna, the ADC is driven by the digitiser

sample clock; the input voltages are critically sampled after passing through an analogue filter for the selected band. The L-band receiver real samples the data at exactly 1712 MHz and passes the second Nyquist zone (i.e., top half of the band 856-1712 MHz) to the correlator-beamformer via optical fibre Ethernet. The digitiser attaches a 48-bit time-stamp to each 10-bit sample. The clock can run for 45 h without overflow - much longer than a typical integration. The 10-bit digitiser offers excellent resistance to radio frequency interference and makes it possible to confine RFI to only the relevant frequency channels unless it causes saturation of the ADC.

Optical timing pulses are generated by the Time and Frequency Reference (TFR) system in the processor building and disseminated to all antennas via dedicated optical fibres. The digitiser records the time of arrival of the optical pulse from the masers; it is also used to reset the digitiser sample clock when necessary. The timing fibres are buried 1 m deep to minimise diurnal temperature variations, but change length over the year as the site temperature varies. A round-trip measurement system continuously measures their length by timing the round trip of the timing pulse as reflected back from the digitiser (Siebrits et al., 2017; Adams et al., 2018). This falls within a general class of time-of-flight measurement which is traceable to the SI unit of time (Terra & Hussein, 2015).

Prior to correlation and beamforming the signals from all antennas are buffered and integer samples of delay are applied to compensate for physical delays. A multi-tap Hann-window polyphase filterbank is used to filter the data along with a phase gradient to eliminate the remaining (sub-sample) geometrical delay. Pulsar timing observations at L-band usually use the 1024 channel mode, giving a time resolution of $1/B$ of 1.196 μs. The narrowest mean MSP profile features are 10s of μs in width although 'giant' pulses have been observed with time resolution from the Crab pulsar with timescales of down to 1 ns (Hankins et al., 2003).

The Precise Time Manager (PTM) is a program that collects and aggregates all known delays in the system: geometric, physical delays in the antenna, analogue and digital delays in the receiver and digitiser, the correlator delay and the digitiser clock offset. PTM computes the *time that the wavefront corresponding to a certain ADC sample crossed the array phase centre*, and the uncertainty in this time. This time is passed to PTUSE for recording in the header of the pulsar observation. In September 2019, the uncertainty in this value was 3 to 4 ns.

2.2.3 Tracking of telescope time: Karoo telescope time

The station clock is referred to as KTT (Karoo Telescope Time). This timescale is generated by the TFR subsystem using an ensemble of two active hydrogen masers, two Rubidium clocks and a quartz crystal. It is a physical timescale, defined at a connector in the system. The masers drift by typically just a few ns per day; KTT is kept $\sim$1 μs from UTC by adjusting their synthesized frequency every few months to keep them in defined offset bands. The TFR also provides accurate time to other components of the telescope via its Precision Time Protocol: this is amongst other things used in the pointing of the telescope and control of the precision timing systems (Adams et al., 2018).

Pulsar timing requires the difference between UTC and KTT to be measured. At MeerKAT, this is done with a set of calculations to calculate ensemble time using interclock differences between five clocks, and measurements of four clocks with respect to GPS via two dual-band GNSS receivers and two single band GPS-only receivers (Burger et al., 2019). The multiple measurements then lead to clock solutions for each of the clocks in the ensemble via linear combinations of the different measurements. The usage of multiple clocks enables error/instability detection in any one of the clocks and a lower variance estimate in any one of the clocks as with standard ensembling used in timescale generation (Levine, 2012).

Reference is made to the UTC via common-view comparison with the National Metrology Institute of South Africa (NMISA) in Pretoria, and by direct comparison with UTC(USNO) via GPS time dissemination. The uncertainty of the absolute time difference between KTT and UTC is specified to be less than 5 ns. At present, the systematic (non-varying) offset is only *stated* to 50 ns due to verification of absolute offset calibration being undertaken. The offset calibration was performed using absolutely calibrated GPS receivers before main observations were being undertaken, and will in future be done using an EMC-quiet calibrator (Gamatham et al., 2018) in order not to disrupt the observations. The repeatability between observations is thought to be about 5 ns, implying that the systematics and the stability will finally converge to the latter number; final absolute calibration via a GPS simulator traceability chain will lower the absolute offset to <1 ns. As we shall see later on, there is evidence from our pulsar timing results that we are approaching these levels of clock correction/stability. Furthermore, the clock tracker is currently being improved from a semi-real time predictive method, to a fully post-facto non-causal filtering type, using Savitzky-Golay filtering (Savitzky & Golay, 1964) on which provisional internal self-consistency checks suggest a numerical error of <1 ns. Post-facto (Levine, 2012), non-causal calculation is always better in improving timing compared to real-time 'UTC-like' timescale estimation, due to an increased data set, administrative oversight, ability to correct for non-idealities and the inherent outperformance of smoothers as compared to

causal filters (Einecke, 2012; Jensen et al., 2012).

2.3 The Polyphase Filterbanks

The MeerKAT channeliser (the F-engine) uses a polyphase filterbank (PFB) to channelise the digitized bandwidth into 1024 or 4096 critically sampled frequency channels with configurations described in Table 1. A PFB filter design with a 16-tap Hann window was deployed aiming to achieve high sensitivity. This design uses only 6dB of attenuation at the channel edges which however gives rise to significant aliasing from adjacent channels. To address this, an alternate 16-tap Hann window design that provides superior spectral purity performance at a modest price in sensitivity (due to reduced effective bandwidth) was implemented. This was achieved by reducing the 6 dB cut-off frequency to 0.91 times the channel width, sacrificing ∼5% of the sensitivity to reduce the leakage by 10 dB.

A comparison between the two modes can be seen in Figure 3, where we plot the total intensity of PSR J1939+2134 for the two filters as a function of frequency and pulse phase - Figures 3a and 3b, and also a difference between an average frequency-dependent profile to highlight the artifacts in Figure 3c. The original filters gave rise to frequency-dependent pulse profiles that possessed 'reflections' of the main and inter-pulses due to spectral leakage from the adjacent channels. This is very bad for precision timing experiments, as depending upon the location of scintillation maxima it can systematically alter the shape of the pulsar's profile and lead to very large systematic errors. The new filter greatly reduces the amplitude of these artifacts which are now seemingly negligible.

2.4 PTUSE: An SKA Pulsar Processing Prototype

PTUSE stands for Pulsar Timing User Supplied Equipment in the standard SARAO nomenclature. This subsystem processes channelised tied-array beam time-series generated by the SARAO beam-formers on high end server class machines. Two machines were deployed for the original development. Each server processed the signal from one of the four potential tied-array beams, and was equipped with 2 NVidia Titan X (Maxwell) graphics cards, 128 GB of RAM, two Intel E5-2623 v3 CPUs, a 40 Gb Mellanox ConnectX network interface card, and 24TB of disk space in a hardware RAID configuration. The server software was developed by Swinburne University of Technology as the pulsar timing prototype system for Square Kilometre Array (SKA) pre-construction.

The servers are connected to a tree of Mellanox 40 Gb switches and receive data in either 4 KB (4096 channel) or 2 KB (1024 channel) UDP packets organized into SPEAD[4] streams. The SPIP[5] software library captures the data from the switch and places it into a ring buffer. The data are split into two sub-bands which are each fully processed in real-time by the DSPSR (van Straten & Bailes, 2011) software library using GPU-accelerated processing pipelines. DSPSR performs coherent dedispersion and can produce folded pulsar profiles (fold mode) or filterbanks (filterbank mode). The fold mode and filterbank mode both support flexible configuration parameters defining the output data resolutions subject to the limits listed in Table 2. UDP capture at the rates required is challenging and the Intel E5-2623 CPUs occasionally drop packets leading to data loss. Rather than have "holes" in the data we process data from the previous cycle of the ring buffer so the system noise level is maintained. This can occasionally replace what should be system noise by a pulse and vice versa. To help eliminate potential artifacts we have now added three new servers to site featuring two Intel Silver 4110/2.1 GHz 8-core CPUs each and dropped packets are now virtually eliminated due to their higher memory bandwidths and other software optimisations. Typical drop rates during 2019 for the L-band data were 700 bytes/minute or less about 4 parts per billion.

Both fold-mode and filterbank-mode data write the sub-banded results to disk in PSRFITS (Hotan et al., 2004) format, which are subsequently combined into a single file and transferred to both the MeerKAT Data Archive and the Swinburne OzSTAR supercomputer. The volume of filterbank data can be extreme when observing at the highest filterbank time resolutions, typical of globular cluster observing, recording data at over 400 MB/s (30 TB/day). These data products may be reduced on machines on-site prior to transfer to the data archive but also copied to future mirror sites planned in Europe (e.g. Max Planck Institute für RadioAstronomie).

PTUSE supports a raw baseband observing mode of the beam-formed data where short segments of raw input data (channelised voltages) that are present in the ring buffer can be slowly written to the disk system. The first generation of hardware could only manage to store <30 s of data in this mode. Recently (Feb 2020) we obtained new servers that stripe 4×2 TB NVME SSD drives together and can in principle record up to 40 minutes of baseband data to disk per server. Baseband mode will enable us to achieve the 1.196 μs time resolution of the polyphase channel bandwidths for the study of giant pulses, pulse microstructure or the timing of many globular cluster pulsars at full time resolution upon playback.

[4] https://casper.ssl.berkeley.edu/wiki/SPEAD
[5] https://github.com/ajameson/spip

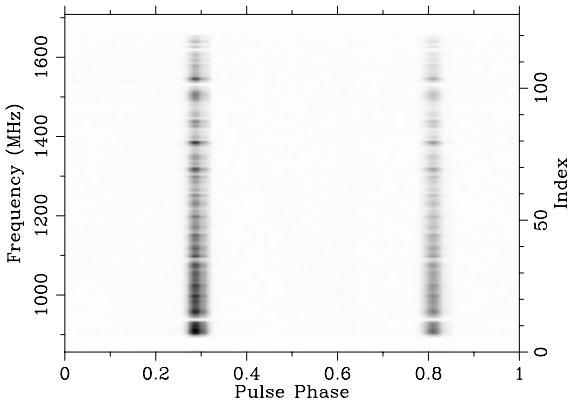

(a) Unmasked with original filter design

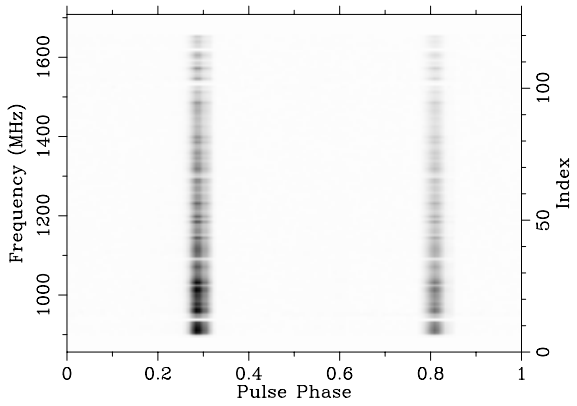

(b) Unmasked with 0.91 filter design

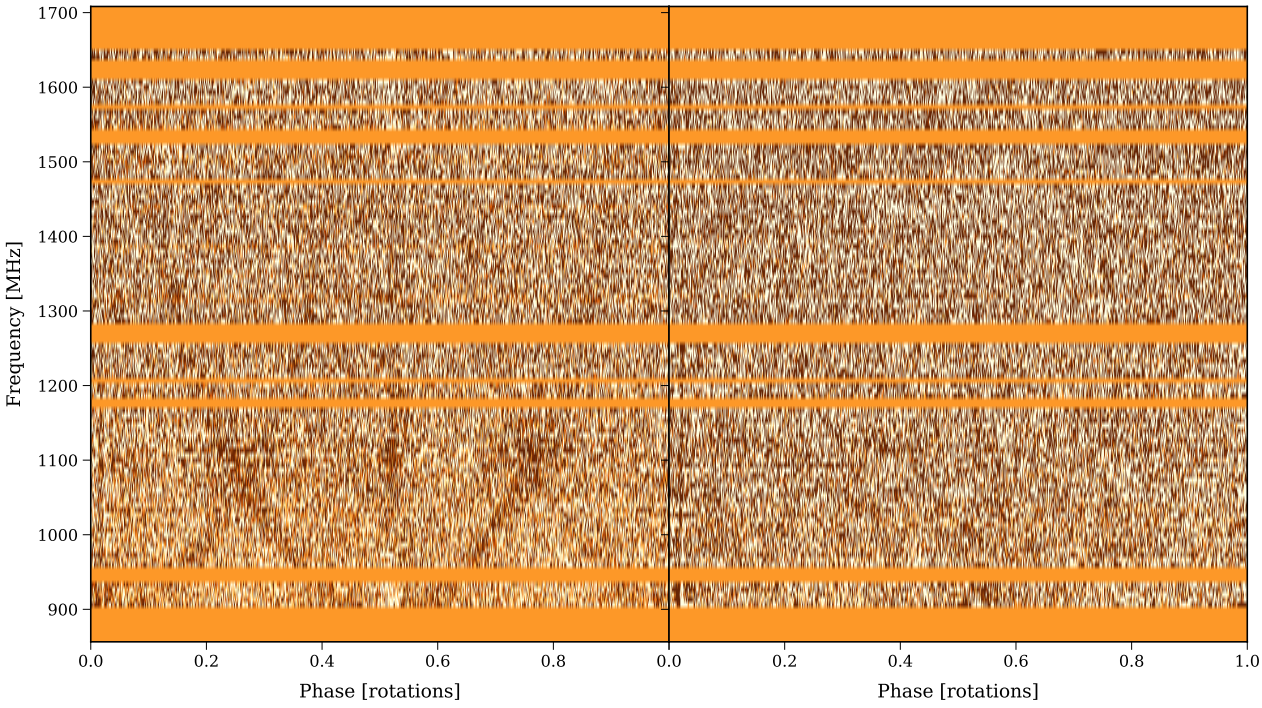

(c) Difference between the pulsar profile and a template with the original filters (left) and the 0.91 filter design (right).

Figure 3. 700-second observations of PSR J1939+2134, coherently dedispersed, folded then integrated into a single profile. The top panels show the total intensity with RFI affected channels masked for the original and 0.91 digital filters applied (see text). The bottom panels show the same profiles after the bright main pulses and weaker interpulse are subtracted using a frequency-dependent mean analytical profile. This reveals the extent of the artifacts that were present in the original filters (left panel of part c) and the extent to which they have been removed (right panel).

Table 1 MeerKAT F-Engine Configurations, with each producing dual polarisations quantised to 8 bits per sample. Frequencies and bandwidths are quoted in MHz and the sampling interval in microseconds.

Band	Approx. Centre Frequency (MHz) †	Bandwidth (MHz)	Channels ($N_{\rm chan}$)	Sampling Interval (μs)	Data Rate (Gbits/s)
L	1284	856	1024	1024/856	27.392
L	1284	856	4096	4096/856	27.392
UHF	816	544	1024	1024/544	17.408
UHF	816	544	4096	4096/544	17.408

† The F-engine PFB implementation lowers the precise centre frequency of all channels by half a fine channel width (i.e. by $BW/N_{\rm chan}/2$), where BW is the total bandwidth. For example, the precise centre frequency of the first channel for L band with 1024 channels is 856 MHz.

Table 2 PTUSE Processing Capabilities

Parameter	Fold Mode	Filterbank Mode	Unit
pulsar ephemeris	catalogue or custom	N/A	
dispersion measure	0 to 2000	0 to 2000	pc cm^{-3}
output phase bins	64 to 4096	N/A	
output polarisation products	1,2 or 4	1,2 or 4	
output sampling interval	N/A	(8 to 1024) * Tsamp	microseconds
output sub-integration length	8 to 60	N/A	seconds
output quantization	16	1, 2, 4 or 8	bits per sample

3 SYSTEM VERIFICATION

3.1 System Equivalent Flux Density

Most pulsars at high dispersion measure (i.e. with DM $> 200\,{\rm pc\,cm^{-3}}$) show little flux density variation at the MeerKAT observing frequencies and can be used to calibrate the system performance. Three such pulsars are PSRs J1602–5100, J1651–4246 and J1809–1917 with flux densities of 7.0, 21.4 and 2.8 mJy at 1369 MHz as measured by the Parkes telescope (Johnston & Kerr, 2018). Each of these pulsars was observed on 4 separate occasions with MeerKAT using the L-band receiver and here we investigate the system performance they imply for the telescope. The data were excised of interference and split into two bands each of 194 MHz centered near 1200 and 1400 MHz in order to best compare with the Parkes data. We derived a system equivalent flux density (including the sky contribution) of 8.1, 8.0, and 10.3 Jy in this central part of the band. It is difficult to accurately estimate the sky contribution with the current MeerKAT system, but the Parkes observations would imply values of 4, 4, and 10 K in the direction of the three pulsars. We therefore conclude that the SEFD is consistent with 7 Jy across 400 MHz of bandwidth.

3.2 Artifacts

To explore the level of any potential system artifacts we compared the pulse profile of the MSP PSR J1939+2134 observed with MeerKAT/PTUSE with archival observations from the CASPSR (CASPER-Parkes-Swinburne-Recorder) coherent dedisperser on the Parkes 64 m radio telescope in the same frequency band. CASPSR digitizes the entire down-converted 400 MHz band and uses the DSPSR library to coherently dedisperse the data using graphics processing units. PTUSE on the other hand dedisperses the narrow polyphase filterbank channels produced by the beamformer using the same software library. There is a danger that each of these methods may create different artifacts in the profile.

PSR J1939+2134 has a steep spectrum and is prone to strong scintillation maxima in narrow (few MHz) frequency bands around 1400 MHz hence it is important to focus on a relatively narrow fractional bandwidth to identify potential artifacts. We selected the relatively narrow bandwidth between 1280 and 1500 MHz at both sites and produced a Stokes I profile for each. As we saw earlier (section 2.3) in some MeerKAT F-engine modes (eg the 4096 channel mode) the spectral leakage is significant between neighbouring channels and the relative heights of the two pulse components from the MeerKAT profile did not agree with the CASPSR data with the weaker of the two pulses being reduced in amplitude by circa 10%. We then repeated the exercise using the new 1K mode of MeerKAT/PTUSE with the sharper filters and found the MeerKAT and Parkes profiles to be consistent within the noise. We attribute this improvement to the choice of filters now in use in MeerKAT's F-engine

that eliminate spectral leakage. This is encouraging for comparisons of pulsar profiles not only between different pulsars at MeerKAT but between observatories that use digital signal processing and common libraries.

3.3 Polarimetry

The boresight polarimetric response of the MeerKAT tied-array beam was estimated using the Measurement Equation Modeling (MEM) technique described in van Straten (2004). Motivated by the results of Liao et al. (2016), the MEM implementation was updated to optionally include observations of an artificial noise source that is coupled after the orthomode transducer (OMT) and to remove the assumption that the system noise has insignificant circular polarisation. The updated model was fit to observations of the closest and brightest MSP, PSR J0437−4715, made over a wide range of parallactic angles, and both on-source and off-source observations of bright calibrator PKS J1934−6342.

The best-fit model parameters include estimated receptor ellipticities that are less than 1° across the entire band, indicating that the degree of mixing between linear and circular polarisation is exceptionally low. The non-orthogonality of the receptors is also very low, as characterised by the intrinsic cross-polarisation ratio (IXR; Carozzi & Woan, 2011), which varies between 50 and 80 dB across the band. Noting that larger values of IXR correspond to greater polarimetric purity, the MeerKAT tied-array beam exceeds both the minimum pre-calibration performance (~ 30 dB; Foster et al., 2015) and the minimum post-calibration performance (~ 40 dB; Cordes et al., 2004; van Straten, 2013) recommended for high-precision pulsar timing.

The reference signal produced by the incoherent sum of the noise diode signals from each antenna significantly deviates from 100% linear polarisation; its polarisation state varies approximately linearly from $\sim 20\%$ circular polarisation at 900 MHz to $\sim 60\%$ circular polarisation at 1670 MHz. Therefore, if an observation of the reference signal were to be used to calibrate the differential gain and phase of the tied-array response, then the technique described in Section 2.1 of Ord et al. (2004) would be necessary.

However, the reference signal also exhibits evidence of a significantly non-linear tied-array response. This is observed as over-polarisation of the reference signal (e.g., degree of polarisation as high as 105% – 110%) and is also observed in the goodness-of-fit (e.g. reduced χ^2 between ∼300 and ∼800) reported when performing MEM with reference source observations included. The origin of the non-linearity is currently not understood; therefore, given that the best-fit values of differential receptor ellipticity are very small[6], all reference source observations (including on-source and off-source observations of PKS J1934−6342) were removed from the MEM input data, yielding good fits to the pulsar signal with reduced χ^2 between ∼1.6 and ∼1.9.

To test the stability of the polarimetric response, observations of PSR J0437−4715 made on 4 September 2019 were modelled and calibrated using MEM and then integrated to form a template with which to model observations made on 3 October 2019 using Measurement Equation Template Matching (METM; van Straten, 2013). The template, formed from an integrated total of 2 hours of observing time, has a signal-to-noise ratio of 3.8×10^4. In each frequency channel that was not flagged as corrupted by RFI, the METM model fit the data well, with reduced χ^2 values ranging between ∼1.1 and ∼1.3. The integrated total of the METM-calibrated data are plotted in Figure 4.

As a final consistency check, the calibrated polarisation of PSR J0437−4715 observed at MeerKAT was quantitatively compared with that observed at the Parkes Observatory using CASPSR. After selecting the part of the MeerKAT band that overlaps with the 400 MHz band recorded by CASPSR, the calibrated MeerKAT data were fit to the calibrated Parkes template using Matrix Template Matching (MTM; van Straten, 2006). The MeerKAT data fit the Parkes data well, with reduced χ^2 values ranging between ∼1.2 and ∼1.5. The Jones matrices that transform the MeerKAT data to the basis defined by the Parkes template in each frequency channel were parameterised using Equation 19 of Britton (2000). All model parameters were close to zero, except for the differential ellipticity, δ_χ, which varied between $+1$ and -2 degrees as a function of frequency, and the rotation about the line of sight, σ_θ, which varied between -5 and -8 degrees. Non-zero values of δ_χ, which describes the mixing between Stokes I and Stokes V, are expected; as described in Appendix B of van Straten (2004), this mixing must be constrained by introducing assumptions that may be correct only to first order. Non-zero values of σ_θ are also expected owing to unmodelled Faraday rotation in Earth's ionosphere.

After initialising the array, a standard operating procedure is to run the so-called delay calibration observation. During the observation, the noise diode as well as bright, well known sources are used to calculate and apply time-variable solutions for the antenna-based delays. The delay calibration observation consists of multiple stages: initially predefined F-engine complex gains are applied in the correlator for each antenna; a suitable calibrator is observed and simple antenna-based delays are calculated; next, a noise diode is activated and cross-polarisation delay as well as phase is measured for the entire array.

[6]Differential receptor ellipticity, which describes the mixing between Stokes I and Stokes V, must be constrained by observations of a source of known circular polarisation, as described in Appendix B of van Straten (2004) and considered in more detail in Liao et al. (2016).

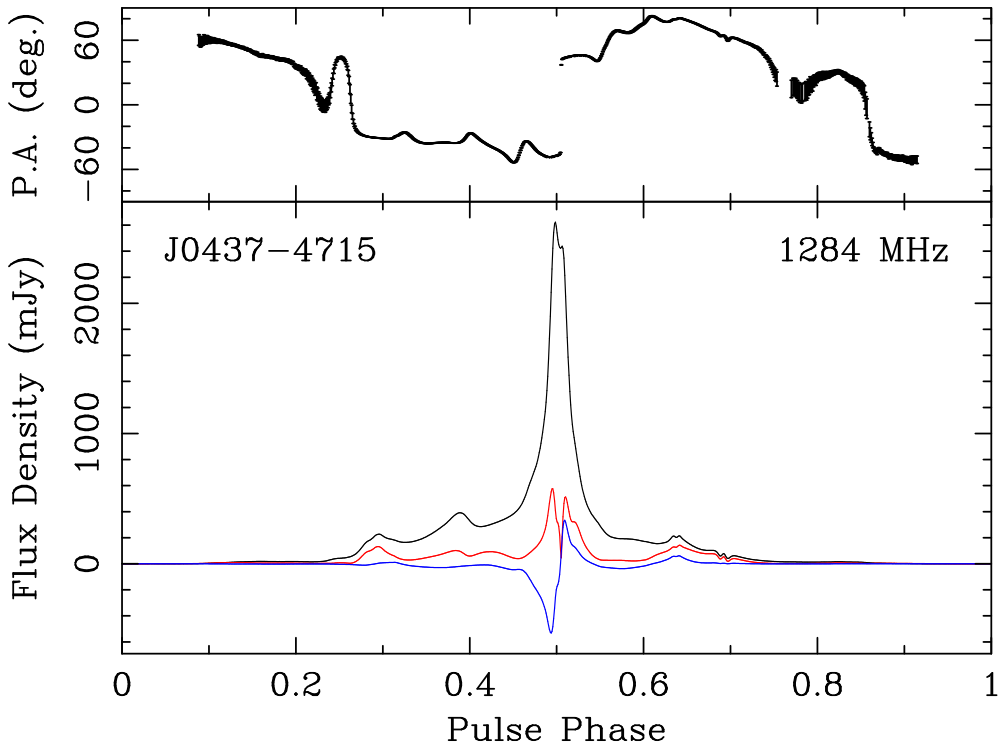

Figure 4. Calibrated polarisation of PSR J0437−4715, plotted as a function of pulse phase. In the top panel, the position angle of the linearly polarized flux is plotted with error bars indicating 1 standard deviation. In the bottom panel, the total intensity, linear polarisation, and circular polarisation are plotted in black, red and blue, respectively.

The delays are derived and combined by the real-time calibration pipeline before being applied to the data with the exception of the cross-polarisation phases which are stored in the observation metadata and can be applied at a later stage.

3.4 Timing

To test the timing stability of the telescope, we routinely observed the bright, narrow MSP PSR J1909−3744 over a period of about 11 months from March 2019.

This pulsar has a well-established ephemeris that we took from the Parkes Pulsar Timing Array (Kerr et al, submitted). We first excised radio frequency interference in the data cube using the COASTGUARD package (Lazarus et al., 2016), which we modified to work with MeerKAT data. Importantly we used frequency-dependent model templates to identify on and off-pulse regions from which to calculate a set of statistics that could be used to identify contaminated profiles that should be excised. We updated the dispersion measure in the data sets to a value near the mean over the observing interval. We then averaged to 32 channels in frequency and completely in time. Using a two-dimensional template, we derived arrival times using the Fourier-domain Monte Carlo method.

We analysed the arrival times using TEMPONEST (Lentati et al., 2014). To first order, MSPs only drift slowly from their timing models, so we started the PPTA ephemeris from its second data release (Kerr et al., submitted) and modelled only the minimum number of additional parameters: the pulsar spin and spin down rate; dispersion measure and first derivative dispersion measure; and the tempo2 FD parameters to account for pulse profile evolution with frequency.

We searched for three forms of stochastic noise in the data. We searched for red noise and DM variations using the established Bayesian methods now commonly employed. To model the white noise we searched for both EQUAD and EFAC (using the temponest definitions), and a new parameter, TECORR, which accounts for correlated white noise, by adding an additional term to the noise covariance matrix

$$\sigma_{ij}^2 = \delta(t_i - t_j)\sigma_{\mathrm{TCORR,hr}}^2\sqrt{3600/T}, \qquad (1)$$

where $\delta(t_i - t_j) = 1$ if the data are from the same integration. The noise parameter is similar to the ECORR that has been employed notably in NANOGrav data analyses. However the noise accounts for varying observing lengths. Correlated noise introduced by stochasticity in pulse shape variations is predicted to reduce in proportion to the square root of time. We find no evidence for red noise in our data set, which is unsurprising given its short length and the steep nature of the red noise in PSR J1909−3744. We find strong evidence for dispersion measure variations, which are visible by eye in our 512-s

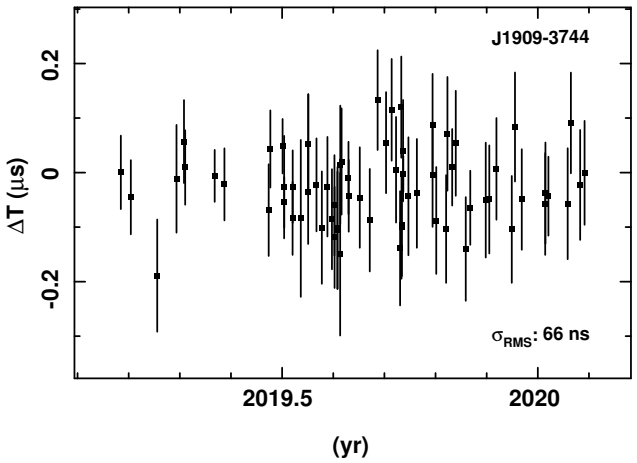

Figure 5. Epoch-averaged residual arrival times for PSR J1909−3744.

observations. We find evidence for band-correlated white noise (TCORR), but no evidence for EQUAD and EFAC. We measure $\sigma_{\rm TCORR,hr} \approx 24$ ns. Which is approximately a factor of two larger than the expected jitter noise measurements inferred from short observations (Shannon et al., 2014). The excess noise is the subject of current research, but we suspect it includes contributions from unmodeled dispersion measure variations (Cordes et al., 2016; Shannon & Cordes, 2017).

After subtracting the maximum likelihood model for dispersion measure variations and forming the weighted average of the sub-banded residual arrival times we found evidence for marginal orbital phase dependent variations in the residuals. After accounting for this by fitting for the companion mass, we measure the root-mean square of the average residual arrival times times to be ≈ 66 ns as shown in Figure 5. Figure 6 shows the residual arrival times plotted versus pulse phase when ignoring entirely (panel a) and accounting for the Shapiro delay caused by the radio waves propagating through the gravitational field of the companion.

To test the timing stability of the system on short timescales, we made use of the bright Fermi source PSR J2241−5236 (Keith et al., 2011). This 2.18 ms MSP has a narrow duty-cycle (∼3%) and is regularly timed as part of the Parkes Pulsar Timing Array. It has a mean 1.4 GHz flux density of 3-4 mJy and often experiences bright scintillation maxima. On April 22 2019 UTC, this pulsar produced a 5030 σ profile in just 512 s in 32 8 s integations. After forming an appropriate smoothed template, we produced arrival times every 8 s after summing over the full bandwidth and obtained an rms residual of the resultant 8 s integrations of only 90 ns using the existing ephemeris. This is the lowest rms residual in 8 s ever seen in pulsar timing and implies a very small jitter upper limit of only $90/(3600/8)^{1/2} = 4.2$ ns in an hour.

Both of these results auger well for the future of MSP

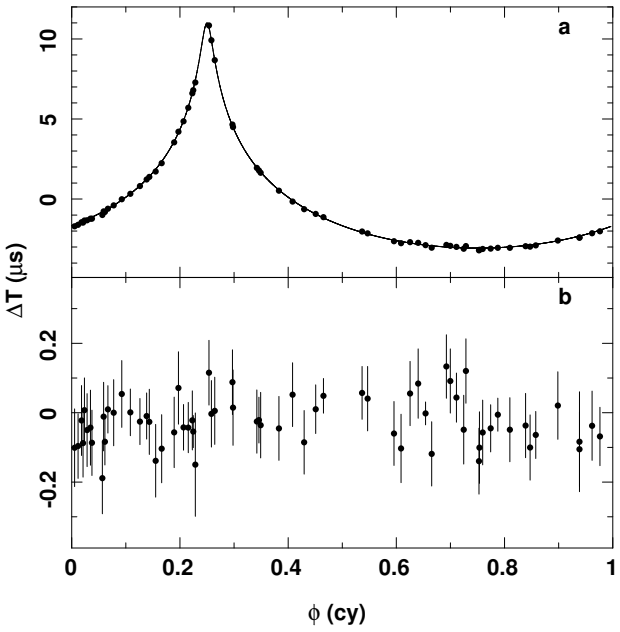

Figure 6. Epoch averaged residual arrival times for PSR J1909−3744 plotted against orbital phase in cycles. Residual arrival times are plotted using the maximum-likelihood model without (panel a) and with accounting for the Shapiro delay induced by the companion. The predicted signal is shown as the solid line in panel a.

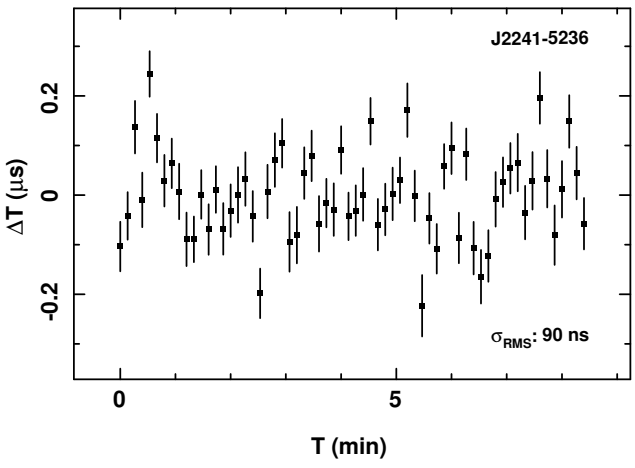

Figure 7. Times of arrival during a 512s observation of PSR J2241–5236 with MeerKAT using the L-band receiver. The post-fit rms residual is just 90 ns using 8-s integrations. This implies a jitter limit of less than 4.2 ns.

timing at the MeerKAT telescope and are a testament to the engineering care that has been achieved with the TFR, PTM and PTUSE.

3.5 Filterbank Mode

The globular cluster Ter 5 was observed in filterbank mode for 2 h on May 27 2019 with 9.57 μs time resolution and full polarimetry. Profiles for the 34 detected pulsars are shown in Figure 8 showing the high time resolution and signal-to-noise ratios for many of the pulsars. These observations only used the central dishes within a 500 m radius of the core to maximise the sensitivity to the pulsars in the arcmin of the core. All pulsars except Ter 5 A, D, X and J were within the half-power point of the beam at the centre frequency of the observation. Ter 5 A is so bright that it was easily detected regardless, but the others were heavily attenuated. The detections of Ter 5 ah and Ter 5 aj are marginal.

Ter 5 O was observed in parallel using the fold-mode of PTUSE and after calibration we derived a rotation measure for the cluster of 174.6±0.8 rad/m^2 which is consistent with the value (178.5±3.5) for the cluster obtained by You et al. (2018) for Ter 5 A. The pulse profile and polarimetry are shown in Figure 9.

4 NEW RESULTS

4.1 A Giant Pulse from PSR J0540–6919

PSR J0540–6919 is a young pulsar in the Large Magellanic Cloud that has been observed by the Parkes telescope to emit giant pulses (Johnston & Romani, 2003) and possesses a twin-peaked average pulse profile (bottom panel Figure 10). In a test of the PTUSE filterbank mode, we observed this source for two hours on March 26 2019 and detected a large number of giant pulses. The brightest giant pulse of peak flux density 5.4 Jy and a mean flux density of 92 mJy is shown in Figure 10. These flux values are estimated using the MeerKAT SEFD values. At its assumed distance (Johnston et al., 2004) of 50 kpc, this giant pulse would have a peak luminosity of 13500 Jy kpc^2. If placed in M31, this giant pulse would have a peak flux of ∼25 mJy and would be detectable by the FAST telescope.

4.2 Nulling in PSR J0633–2015

The raw sensitivity of MeerKAT makes it ideal to study single pulse phenomenology in large number of pulsars previously too weak for such studies. For example, understanding the population and characteristics of nulling pulsars, and how the pulsar sets the timescale for the on- and off-periods are key questions of the emission physics. PSR J0633−2015 is a long period pulsar discovered by (Burgay et al., 2006) who made no mention of

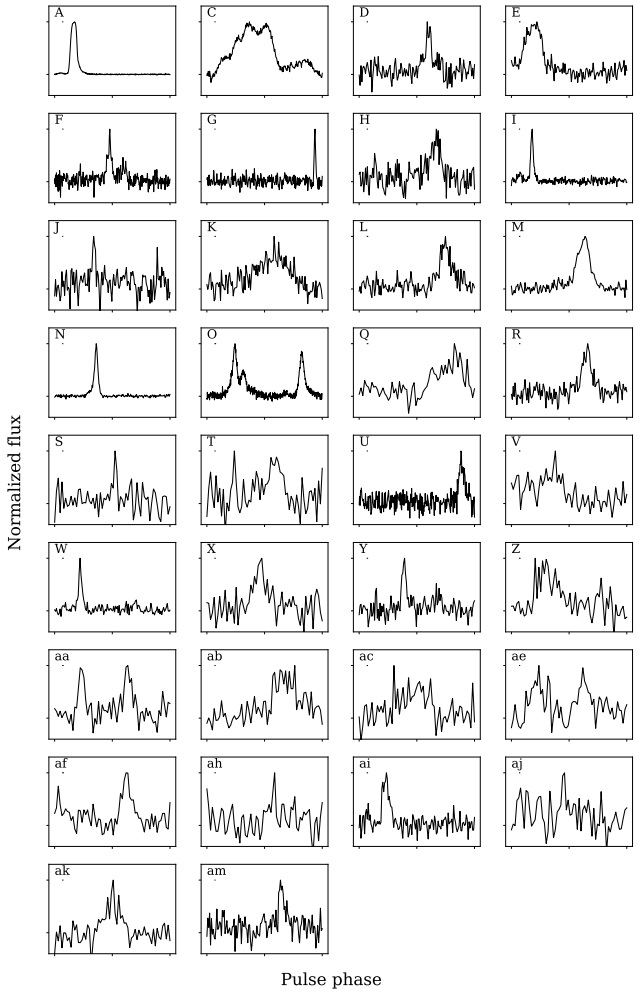

Figure 8. Folded pulse profiles of the 34 pulsars in Terzan 5 from a 9000 s integration.

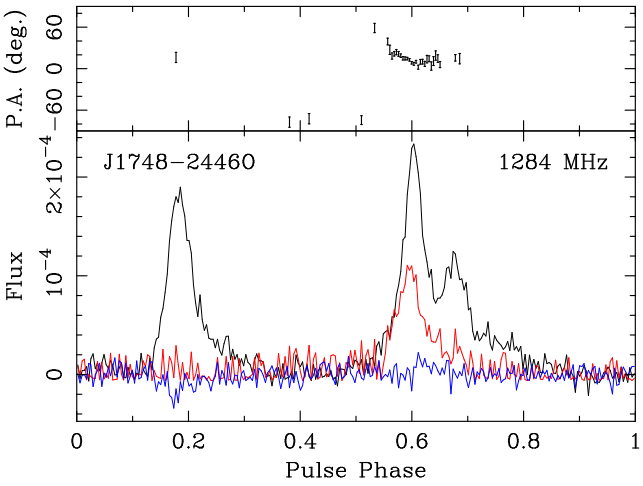

Figure 9. Calibrated polarisation profile of PSR J1748−2446O, plotted as a function of pulse phase. In the top panel, the position angle of the linearly polarized flux is plotted with error bars indicating 1 standard deviation. In the bottom panel, the total intensity, linear polarisation, and circular polarisation are plotted in black, red and blue, respectively.

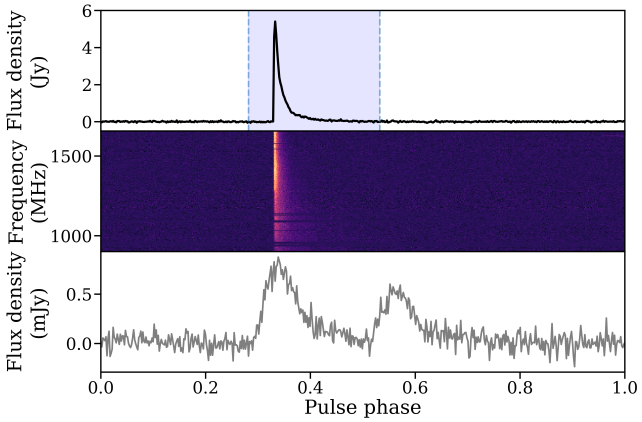

Figure 10. *Top and middle:* Giant pulse from PSR J0540−6919 with a peak flux density of 5.4 Jy and an estimated mean flux density of ∼ 92 mJy. Using the SEFD of MeerKAT the off-pulse rms is estimated to be 20 mJy. The shaded region in the top panel shows the selected on-pulse region. The pulsar at these frequencies is subject to scattering that gives rise to the exponential tail. *Bottom:* The averaged 2 hr pulse profile.

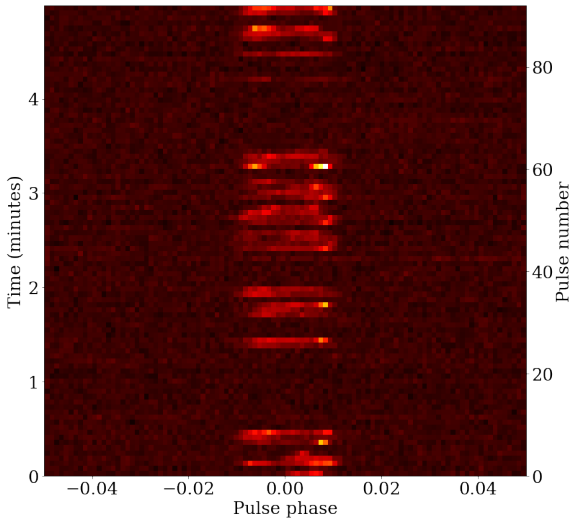

Figure 11. Short term nulling in PSR J0633−2015 in observations made on 2019 October 27. Each horizontal row shows an individual pulse, with the colour coding denoting the flux density of the pulsar.

its unusual pulse-pulse characteristics. Figure 11 shows a 5 minute observation made with MeerKAT on 2019 October 27. Each horizontal row shows a colour-coded representation of the flux density each individual pulse from the pulsar. Short duration nulling is clearly visible.

4.3 Double Pulsar Timing

A full orbit of the double pulsar PSR J0737−3039A (Burgay et al., 2003; Lyne et al., 2004) was observed to assess the precision of its arrival times with MeerKAT using 56 antennas. Using 16 × 53.5 MHz sub-bands and 64 s integrations we obtained a post-fit rms residual of just 9.3 μs. Averaging across the full band yields a post-fit arrival time rms of just 2.3 μs in 64 s. By comparison, a 2013 archival observation of J0737−3039A with the Parkes 64 m telescope using the multibeam receiver and the 340 MHz CASPSR coherent dedisperser 64 s integrations yielded 15 μs rms residuals. The improvement in timing is therefore a factor of 6.5.

We now examine how this compares with the radiometer equation expectations? The SEFD of the Parkes telescope/multibeam receiver is ∼ 30 Jy whereas MeerKAT is ∼7 Jy and the effective (RFI-free) bandwidths used are 340 and ∼756 MHz respectively. Therefore, we would expect the ratio of the MeerKAT residuals to that of the Parkes multibeam CASPSR residuals to be of order $56/64 \times 7/30 \times \sqrt{340/756} \sim 1/7$, in good agreement with our measured ratio of 6.5. Given the flux density variations exhibited by pulsars at the dispersion measure of this pulsar (48.9 pc cm^{-3}) due to interstellar scintillation this is perfectly consistent with expectations based on our impressive telescope gain and system temperature figures quoted for MeerKAT's L-band receiver. A factor of 6.5 in timing residuals increases observing efficiency by a factor of $6.5^2 \sim 40$.

These test observations imply that MeerKAT will be important for studies of the double pulsar, in particular its eclipse, Shapiro delay, and hunts for the (now invisible) "B" pulsar that demand high sensitivity (see e.g. Lorimer & Kramer, 2004). In the longer term, extremely high precision will be required to separate the contributions of Lense-Thirring precession to the relativistic advance of periastron and hence determine the moment of inertia of the neutron star in a novel way.

5 DISCUSSION AND OUTLOOK

The MeerKAT telescope was designed both to be a powerful standalone instrument and to be integrated into SKA1-mid in the mid 2020s. The development and commissioning of the PTUSE instrument has demonstrated that it is achieving excellent sensitivity, pulsar timing and polarimetric accuracy and already making discoveries such as new records on pulse jitter and timing stability. But MeerKAT has the potential to break other new ground. It is an extremely agile mechanical telescope, and can slew at 2 deg/s in azimuth and 1 deg/s in elevation. The current dead time between pulsar observations is now just ∼5 s leading to high observing efficiencies. In many regions of the galaxy, many pulsars will occupy the same primary beam, and in future array releases it will be possible to place a tied-array beam on up to four objects at once to further enhance the timing program efficiency. However other opportunities exist to further enhance pulsar timing at MeerKAT. The TRAPUM and Breakthrough Listen compute clusters

currently being commissioned on site receive the voltages from every individual antenna and can form coherent beams that can be independently steered within the primary beam. TRAPUM will form up to (depending upon bandwidth) 900 coherent beams to search for pulsars and Fast Radio Bursts whilst the Breakthrough cluster intends to search for techno-signatures from advanced civilisations. These instruments can complement PTUSE by placing a tied beam on all known pulsars within the primary beam to maximise efficiency when timing the dozens of MSPs that inhabit globular clusters like 47 Tucanae and Terzan 5.

In February 2020, additional copies of the PTUSE machine were installed and four completely independent sub-arrays were tested, each of them observing a different pulsar. It will soon be possible to time over 1000 pulsars in just an 8 hour period using these modes.

All of the low dispersion measure MSPs ($DM < 40$ pc cm^{-3}) exhibit scintillation maxima on the timescale of hours that can easily amplify/deamplify their mean flux by factors of several. If we could observe MSPs during such maxima the benefits in observing efficiency are great. In the absence of limits from pulse jitter, a factor of just two in mean flux density is worth a four-fold improvement in timing efficiency according to the radiometer equation. Hence in the future we intend to use the bulk of the array to time a timing array MSP whilst a small group of antennas conduct an audit of potential targets that may be in a bright scintillation state. This could lead to dramatic increases in the sensitivity of the MeerKAT pulsar timing array and its contribution to the IPTA's goal of detecting nanoHz gravitational waves.

The MeerTime Large Survey Project consists of four major sub-projects or themes: relativistic and binary pulsars, globular clusters, the MeerTime Pulsar Timing Array and the Thousand Pulsar Array. These all aim to create a legacy dataset for current and future generations of astronomers. Data on the first three projects will be made available 18 months after observations are completed or upon publication. The Thousand Pulsar Array (Johnston, 2020) has an ambitious objective to make its data public once it is cleaned, calibrated, and the timing corrections are secure. As of Feb 26 2020 MeerTime[7] has already observed 1005 unique target pulsars in 825 h of observing and shows that MeerKAT should be an exceptional pulsar facility in the lead-up to its incorporation into the SKA. Many of the pointings were of globular clusters, and hence well over 1000 individual pulsars have already obtained pulse profiles suitable for timing and polarimetry.

[7] www.meertime.org

6 ACKNOWLEDGEMENTS

Parts of this research were conducted by the Australian Research Council Centre of Excellence for Gravitational Wave Discovery (OzGrav), through project number CE170100004. FJ acknowledges funding from the European Research Council (ERC) under the European Union's Horizon 2020 research and innovation programme (grant agreement No. 694745). AS and JvL acknowledge funding from the Netherlands Organisation for Scientific Research (NWO) under project "CleanMachine" (614.001.301). YM, AS and JvL acknowledge funding from the ERC under the European Union's Seventh Framework Programme (FP/2007-2013) / ERC Grant Agreement n. 617199. A. Ridolfi gratefully acknowledges financial support by the research grant "iPeska" (P.I. Andrea Possenti) funded under the INAF national call PRIN-SKA/CTA approved with the Presidential Decree 70/2016. Pulsar research at the Jodrell Bank Centre for Astrophysics is supported by a consolidated grant from the Science and Technology Facilities Council (STFC). The National Radio Astronomy Observatory is a facility of the National Science Foundation operated under cooperative agreement by Associated Universities, Inc. SMR is a CIFAR Fellow and is supported by the NSF Physics Frontiers Center award 1430284. Pulsar research at UBC is supported by an NSERC Discovery Grant and by the Canadian Institute for Advanced Research. The MeerKAT telescope is operated by the South African Radio Astronomy Observatory, which is a facility of the National Research Foundation, an agency of the Department of Science and Innovation. MeerTime data is housed on the OzSTAR supercomputer at Swinburne University of Technology. The MeerTime Pulsar Timing Array acknowledges support of the Gravitational Wave Data Centre funded by the Department of Education via Astronomy Australia Ltd. MK and DCJ acknowledge significant support from the Max-Planck Society (MPG). PTUSE was developed with support from the Australian SKA Office and Swinburne University of Technology.

REFERENCES

Adams G., et al., 2018, in 2018 IEEE International Frequency Control Symposium (IFCS). IEEE, doi:10.1109/FCS.2018.8597533

Bailes M., et al., 2018, arXiv e-prints, p. arXiv:1803.07424

Britton M. C., 2000, ApJ, 532, 1240

Burgay M., et al., 2003, Nature, 426, 531

Burgay M., et al., 2006, MNRAS, 368, 283

Burger J., Siebrits R., van Tonder V., Adams G., Welz M., Ramudzuli Z., Kapp F., 2019, in du Plessis M., ed., Vol. 11043, Fifth Conference on Sensors, MEMS, and Electro-Optic Systems. SPIE, pp 425 – 448, doi:10.1109/FCS.2016.7563589

Camilo F., et al., 2018, ApJ, 856, 180

Carozzi T. D., Woan G., 2011, IEEE Transactions on Antennas and Propagation, 59, 2058

Cordes J. M., Kramer M., Lazio T. J. W., Stappers B. W., Backer D. C., Johnston S., 2004, New Astron.

Rev., 48, 1413
Cordes J. M., Shannon R. M., Stinebring D. R., 2016, ApJ, 817, 16
Dai S., et al., 2015, MNRAS, 449, 3223
DeBoer D. R., et al., 2017, PASP, 129, 045001
Dewdney P. E., Hall P. J., Schilizzi R. T., Lazio T. J. L. W., 2009, IEEE Proceedings, 97, 1482
Einecke G. A., 2012, Smoothing, Filtering and Prediction: Estimathing the Past, Present and Future. Intech, Janeza Trdine 9, 51000 Rijeka, Croatia
Foster G., Karastergiou A., Paulin R., Carozzi T. D., Johnston S., van Straten W., 2015, MNRAS, 453, 1489
Gamatham R., et al., 2018, in 2018 IEEE International Frequency Control Symposium (IFCS). IEEE, doi:10.1109/FCS.2018.8597563
Hankins T. H., Kern J. S., Weatherall J. C., Eilek J. A., 2003, Nature, 422, 141
Hobbs G., et al., 2019, arXiv e-prints, p. arXiv:1911.00656
Hotan A. W., van Straten W., Manchester R. N., 2004, PASA, 21, 302
Jankowski F., van Straten W., Keane E. F., Bailes M., Barr E. D., Johnston S., Kerr M., 2018, MNRAS, 473, 4436
Jensen J. R., Benesty J. Christensen M. G., Jensen S. H., 2012, IEEE Transactions on Audio, Speech, and Language Processing, 20, 1526
Johnston S. e. a., 2020, MNRAS
Johnston S., Kerr M., 2018, MNRAS, 474, 4629
Johnston S., Romani R. W., 2003, ApJ, 590, L95
Johnston S., Romani R. W., Marshall F. E., Zhang W., 2004, MNRAS, 355, 31
Keith M. J., et al., 2011, MNRAS, 414, 1292
Kramer M., et al., 2016, in MeerKAT Science: On the Pathway to the SKA. p. 3
Lazarus P., Karuppusamy R., Graikou E., Caballero R. N., Champion D. J., Lee K. J., Verbiest J. P. W., Kramer M., 2016, MNRAS, 458, 868
Lentati L., Alexander P., Hobson M. P., Feroz F., van Haasteren R., Lee K. J., Shannon R. M., 2014, MNRAS, 437, 3004
Levine J., 2012, Review of Scientific Instruments, 83
Liao Y.-W., Chang T.-C., Kuo C.-Y., Masui K. W., Oppermann N., Pen U.-L., Peterson J. B., 2016, ApJ, 833, 289
Liu K., Keane E. F., Lee K. J., Kramer M., Cordes J. M., Purver M. B., 2012, MNRAS, 420, 361
Lorimer D. R., Kramer M., 2004, Handbook of Pulsar Astronomy. Vol. 4
Lyne A. G., et al., 2004, Science, 303, 1153
Manchester R. N., Hobbs G. B., Teoh A., Hobbs M., 2005, AJ, 129, 1993
Manchester R. N., et al., 2013, PASA, 30, e017
Maron O., Kijak J., Kramer M., Wielebinski R., 2000, A&AS, 147, 195
Ng C., et al., 2015, MNRAS, 450, 2922
Ord S. M., van Straten W., Hotan A. W., Bailes M., 2004, MNRAS, 352, 804
Osłowski S., van Straten W., Hobbs G. B., Bailes M., Demorest P., 2011, MNRAS, 418, 1258
Perera B. B. P., et al., 2019, MNRAS, 490, 4666
Savitzky A., Golay M. J. E., 1964, Anal.Chem, 36, 1627
Shannon R. M., Cordes J. M., 2017, MNRAS, 464, 2075
Shannon R. M., et al., 2014, MNRAS, 443, 1463
Siebrits R., et al., 2017, in du Plessis M., ed., Vol. 10036, Fourth Conference on Sensors, MEMS, and Electro-Optic Systems. SPIE, pp 325 – 330, doi:10.1117/12.2245776
Taylor J. H., 1992, Philosophical Transactions of the Royal Society of London Series A, 341, 117
Terra O., Hussein M., 2015, Journal of Optical Communications, 37, 187
Toscano M., Bailes M., Manchester R. N., Sand hu J. S., 1998, ApJ, 506, 863
Weisberg J. M., Huang Y., 2016, ApJ, 829, 55
You X. P., Manchester R. N., Coles W. A., Hobbs G. B., Shannon R., 2018, ApJ, 867, 22
van Straten W., 2004, ApJS, 152, 129
van Straten W., 2006, ApJ, 642, 1004
van Straten W., 2013, ApJS, 204, 13
van Straten W., Bailes M., 2011, PASA, 28, 1
van Straten W., Bailes M., Britton M., Kulkarni S. R., Anderson S. B., Manchester R. N., Sarkissian J., 2001, Nature, 412, 158